Robust Estimation Approach for Blind Denoising

Tamer Rabie, *Senior Member, IEEE*

***Abstract*—This work develops a new robust statistical framework for blind image denoising. Robust statistics addresses the problem of estimation when the idealized assumptions about a system are occasionally violated. The contaminating noise in an image is considered as a violation of the assumption of spatial coherence of the image intensities and is treated as an outlier random variable. A denoised image is estimated by fitting a spatially coherent stationary image model to the available noisy data using a robust estimator-based regression method within an optimal-size adaptive window. The robust formulation aims at eliminating the noise outliers while preserving the edge structures in the restored image. Several examples demonstrating the effectiveness of this robust denoising technique are reported and a comparison with other standard denoising filters is presented.**

***Index Terms*—Blind denoising, Gaussian noise filtering, image restoration, outliers, redescending estimators, robust denoising, robust statistics.**

I. Introduction

IMAGES are likely to be degraded by the sensing environment when acquired through optical, electrooptical, or electronic means. The degradation may be in the form of sensor noise, blur due to camera misfocus, relative object-camera motion, random atmospheric turbulence, etc. For digitally acquired pictures, noise can be summarized as the visible effects of an electronic error in the final image. Noise is a function of how well the image sensor and digital signal processing systems inside a digital camera are prone to and can cope with or remove these errors. Noise significantly degrades the image quality and increases the difficulty in discriminating fine details in the image. It also complicates further image understanding and low-level computer vision processing, such as image segmentation and edge detection. The type of high-ISO sensor noise produced by a typical digital camera charge-coupled device (CCD) imaging sensor can be modeled as an additive white Gaussian distribution [1]–[3] with zero mean and a variance (noise power) that can be estimated from the degraded image.

In general, noise can be considered as a violation of the assumption of spatial coherence of the image intensities. In particular, imaging model violations such as these result in picture measurements that can be viewed in a statistical context as outliers. Thus, arises the need for image denoising. This problem can be treated as one of recovering an ideal picture in the presence of these outliers, and, hence, we appeal to the field of robust statistics which addresses the problem of estimation when idealized assumptions about the system will occasionally be violated [4]–[6].

In the following sections, a detailed account of a simple method for blind image denoising using robust statistics is introduced with experimental results showing its effectiveness at restoring Gaussian noise degraded images.

II. Image Denoising

Statistical characteristics of images are of fundamental importance in many areas of image processing. Incorporation of *a priori* statistical knowledge of spatial correlation in an image, in essence, can lead to considerable improvement in many image processing algorithms. For noise filtering, the well-known Wiener filter (after Wiener, who first proposed the concept in 1942 [7]) for minimum mean-square error (MMSE) estimation is derived from a measure or an estimate of the power spectrum of the image, as well as the transfer function of the spatial degradation phenomenon and the noise power spectrum [8]. Unfortunately, the Wiener filter is designed under the assumption of wide-sense stationary signal and noise (a stochastic process is said to be stationary when its statistical characteristics are spatially invariant [9]). Although the stationarity assumption for additive, zero-mean, Gaussian white noise is valid for most cases, it is not reasonable for most realistic images. What this means in the case of the Wiener filter is that we will experience uniform filtering throughout the image, with no allowance for changes between busy and flat regions, resulting in unacceptable blurring of fine detail across edges and inadequate filtering of noise in relatively flat areas.

Noise reduction filters have been designed in the past with this stationarity assumption. These have the effect of removing noise at the expense of signal structure. Examples such as the fixed-window Wiener filter and the fixed-window mean and median filters have been the standard in noise smoothing for the past three decades [8], [10], [11]. These filters typically smooth out the noise, but destroy the high-frequency structure of the image in the process. This is mainly due to the fact that these filters deal with the fixed-window region as having sample points that are stationary (belonging to the same statistical ensemble). For natural scenes, any given part of the image generally differs sufficiently from the other parts so that the stationarity assumption over the entire image or even inside a fixed-window region is not generally valid. The attention of researchers has, thus, been focused during the past two or more decades on developing nonlinear adaptive denoising algorithms that take into account the nonstationarity nature of most realistic images [12]–[18].These nonlinear methods have been used as an alternative to preserve signal structure as much as possible. Many, however, do this at the expense of proper noise reduction, where the high-fre-

Manuscript received February 3, 2004; revised November 2, 2004. This work was supported by the Natural Sciences and Engineering Research Council of Canada through an NSERC Discovery Grant. The associate editor coordinating the review of this manuscript and approving it for publication was Prof. Vicent Caselles.

The author is with the Intelligent Transportation Systems Centre, University of Toronto, Toronto, ON M5S 1A4, Canada (e-mail: tamer@cs.utoronto.ca).

Digital Object Identifier 10.1109/TIP.2005.857276

quency areas will be insufficiently filtered, which will result in a large amount of high-amplitude noise remaining around edges in the image. One class of nonlinear estimation techniques that are gaining popularity for the problem of image denoising are the *robust estimation-based filters* which draw their mathematical basis from the field of robust statistics. Robust statistics filtering has been adapted for image denoising in the early work of Kashyap and Eom [19], who develop a robust parameter estimation algorithm for an image model that contains a mixture of Gaussian and impulsive noise. They assume that their image model is locally stationary and, thus, divide the image into fixed windows and apply their robust estimation algorithm for each window with results that compare favorably against standard denoising methods. Recent work involving robust statistics-based image denoising include work by Hamza and Krim [20], Sardy *et al.* [21], and Ponomaryov *et al.* [22]. Hamza and Krim propose three filtering schemes; the mean-median filter, the mean-relaxed median filter, and Mean-Log-Cauchy filter, while Sardy *et al.* propose wavelet-based estimators using a robust loss function, and Ponomaryov *et al.* design a filter based on redescending M-estimators combined with median estimators to provide impulsive noise rejection. These methods show promising experimental results at filtering heavy-tailed and mixed noise. In contrast, our technique described in this work is primarily concerned with denoising medium to low severity Gaussian white noise-degraded natural images.

In related work on robust anisotropic diffusion [23], Black *et al.* use robust estimation to deal with intensity discontinuities in natural images and apply their robust formulation to smooth the noisy image while assuming the only outliers in the image are those due to the intensity discontinuities. This is in constrast to our method which deals with the intensity discontinuities using an optimal-size adaptive windowing framework, which will be discussed in Section IV, and assumes the outliers are only due to the noise itself, thus facilitating its removal, as will be shown in the experimental results of Section V. Other nonlinear anisotropic diffusion techniques [24]–[27] have been widely studied for the application of image denoising since the early work of Perona and Malik [28], [29] whose method we will use as a comparison with our technique due to its availabity in the public domain.

Another related denoising technique by Tomasi and Manduchi [30] is bilateral image filtering, where a noniterative edge-preserving smoothing hybrid filter is proposed which combines both domain and range filtering, with the range filtering component acting as an adaptive windowing technique. Also, a connection between robust anisotropic diffusion, bilateral filtering, and adaptive windowing has been established in recent work by Barash and Comaniciu [31], with typically similar results to those obtained from both [23] and [30].

In the remainder of this paper, we take a close look at the problem of recovering natural images degraded by Gaussian white noise when the observed image model differs statistically from a stationary model. We propose a, relatively simple but sound, robust statistics-based denoising algorithm that will be shown to be highly effective at restoring images degraded by Gaussian white noise at varying degrees of severity while preserving vital image structure to the highest degree.

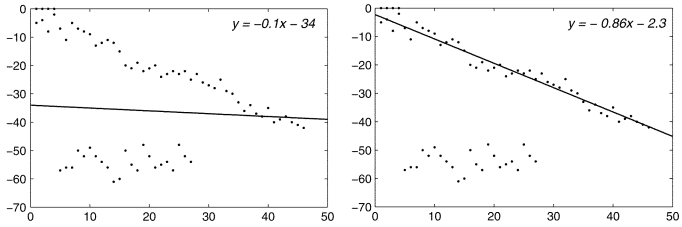

Fig. 1. Left: Least-squares line fit is affected by the outlier data points and produces an inaccurate fit to the majority of the data. The estimated equation of this least-squares line is $y = -0.1x - 34$. Right: Robust estimation gives a more accurate line fit, with equation $y = -0.86x - 2.3$.

III. Robust Statistics

The field of robust statistics [6], [5] was developed to address the fact that the parametric models of classical statistics are often approximations of the phenomena being modeled. In particular, the field addresses how to handle outliers, or gross errors, which do not conform to the assumptions [32].

More precisely, robust statistics addresses the problem of finding the best fit of a model $\mathbf{f} = \{f_0, f_1, \ldots, f_{S-1}\}$ to a set of data measurements, $\mathbf{g} = \{g_0, g_1, \ldots, g_{S-1}\}$,in cases where the data differs statistically from the model assumptions. In fitting a model, the goal is to find the values of $\mathbf{f}$ that minimize the size of the residual errors $(\mathbf{g} - \mathbf{f})$. This minimization can be written as

$$\min \sum_{s \in S} \rho((g_s - f_s), \sigma) \tag{1}$$

where σ is a scale parameter, and ρ is an estimator function. When the errors in the measurements are Gaussian distributed, the optimal estimator is the quadratic estimator [32] given by

$$\rho(x, \sigma) = \frac{x^2}{2\sigma^2} \tag{2}$$

which, when used in the above minimization, reduces the problem to the standard least-squares estimation. The function ρ is called an M-estimator because it corresponds to the maximum-likelihood estimate. The robustness of an estimator refers to its tolerance to outliers (i.e., insensitivity to deviations from the assumed statistical model).

A rough, but useful, measure of robustness is the *breakdown value* [33], which is the largest percentage of outlier data points that will not cause a deviation in the solution. The least-squares approach has a breakdown value of 0% because introducing a single outlier in the data sample will cause a deviation in the estimate from the desired solution. A robust estimator, however, may have a breakdown value of up to 50%. Fig. 1 shows an example of fitting a line to data samples in the presence of outliers. It is clear that the least-squares fit in Fig. 1(left) is inclined toward the outliers, while the robust fit in Fig. 1(right) gives a more accurate fit to the majority of the data samples and rejects the outliers.

A second measure of robustness is the influence function [6], [5] which is the change in an estimate caused by insertion of outlying data as a function of the distance of the data from the (uncorrupted) estimate. For example, the influence function of the least squares estimator is simply proportional to the distance of the data point, $\mathbf{g}$, from the model $\mathbf{f}$. Fig. 2 shows a plot of

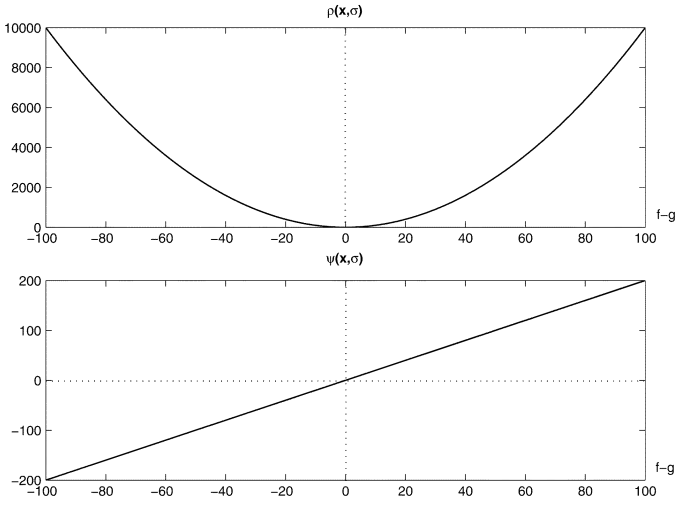

Fig. 2. Top: Quadratic Estimator ρ for $\sigma = 1/\sqrt{2}$. Bottom: Its influence function ψ.

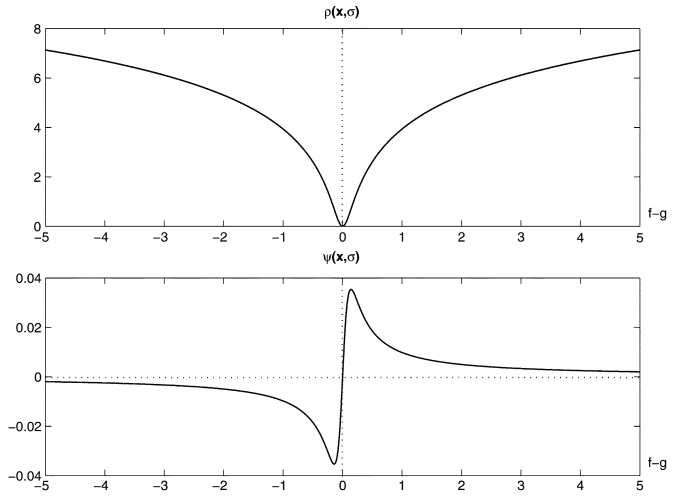

Fig. 3. Top: Lorentzian Robust Estimator ρ. Bottom: Its influence function ψ.

the quadratic estimator in (2) (for $\sigma = 1/\sqrt{2}$) as a function of the distance $\mathbf{f} - \mathbf{g}$ (top plot). The influence function (bottom plot) is the derivative of the estimator and clearly shows that the influence of outliers increases linearly.

To achieve robustness, we consider *redescending* estimators [6] for which the influence function tends to zero with increasing distance. We follow the example of Black and Rangarajan, for reconstructing a smooth surface from noisy depth data using robust statistics, and choose the Lorentzian robust estimator for being continuously differentiable, and for having a redescending influence function which has a simple form [34], [23]. Fig. 3 shows a plot of both the Lorentzian robust estimator and its influence function which clearly shows its redescending behavior for which the influence of outliers tends to zero.

IV. Robust Denoising Filter

We now apply the tools of robust statistics to develop a framework for the robust estimation of the ideal image signal when the only information we have is the corrupted observed image. This robust formulation is based on a simple idea of rejecting outlier pixels (noise pixels) appearing in the corrupted image that do not belong to the ensemble of samples in an adaptive window around the pixel of interest. In formulating our robust denoising filter we use an observed image model with additive noise as follows:

$$\mathbf{g} = \mathbf{f} + \mathbf{n} \tag{3}$$

where $\mathbf{n}$ is a zero-mean additive white Gaussian noise random variable, of variance $\sigma^2_{\mathbf{n}}$, and uncorrelated to the (unknown) ideal image $\mathbf{f}$, which is assumed to be of nonzero mean, $m_{\mathbf{f}}$, and variance $\sigma^2_{\mathbf{f}}$, and $\mathbf{g}$ is the observed noise-corrupted image of nonzero mean, $m_{\mathbf{g}} = m_{\mathbf{f}}$, and variance $\sigma^2_{\mathbf{g}}$.

For the purpose of the following analysis, we make basic assumptions about our estimated image model $\hat{\mathbf{f}}$ as being of the wide-sense stationary type, with a spatially coherent content (i.e., no contaminating noise of any kind and smooth transitions in the values of its pixels with a signal standard deviation $\sigma_{\hat{f}} \leq \epsilon$, where ϵ is a spatially invariant constant). We also add the assumption that both the ideal image f_s and the additive noise frame n_s, $s \in [0, S-1]$ for an S-sized image, are ergodic random variables. The implications of this latter assumption is that although we do not have *a priori* knowledge of the signal and noise statistical variance and mean, we can still capture samples of f_s and n_s and determine their variance and mean, which are, in turn, representative of their respective ensembles. It should also be noted that although the noise variance, σ^2_n, is not known *a priori*, it is easily estimated from a window in a flat area of the degraded image g_s [35].

Our approach is to compute a denoised signal estimate by minimizing a stationarity cost function E that enforces the first assumption about our estimate (i.e., spatial coherence) and constrains image intensities at a particular location, s, to belong to the ensemble of neighborhood samples, N. Typically, N is chosen to be the 4-connected or 8-connected neighborhood of the pixel being processed [34], [23]. Using such fixed-size neighborhood regions restricts the analysis window to small sizes due to the danger of a larger-sized window crossing over image boundaries in which computed statistics will be poor representations of the true local estimates. The shortcomings of using small window sizes is the lack of enough samples to give an accurate estimate of the local statistics.

An obvious alternative is to use an adaptive analysis window. This adaptive window is to be formed such that it includes relatively uniform structures in the ideal image, so that the primary source of variance in the window is the additive noise. In developing an effective adaptive window to account for the nonstationarity of images, it is important for this analysis window to have the maximum size possible at each pixel position without crossing over image structure and edges. The reason is that the more the number of spatially correlated signal samples are available in the analysis the more accurate their statistical characteristics can be estimated [36]. Previous adaptive windowing techniques are not "optimal" in this respect as they usually vary the window size in the right-most upper quadrant only; namely the positive x axis and the positive y axis, and simply duplicate these values in the negative axis. Thus, the window grows in size symmetrically, increasing to the maximum (user-preset) allowable size $N_{\max}$ in the middle of a flat region of the image

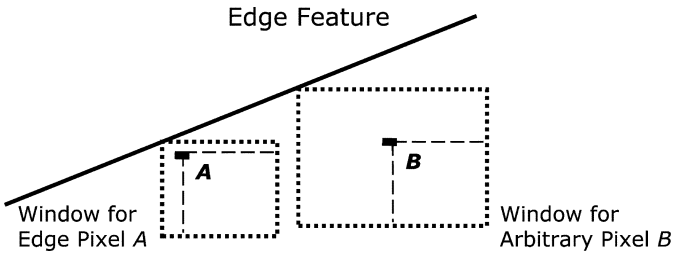

Fig. 4. Optimal-size windowing. For each individual pixel, the window size is allowed to grow large, even for edge pixels, but does not cross over neighboring edges.

and decreasing to the minimum size (usually just a single pixel) near the edges [16], [37]. This causes severe statistical errors near edge regions.

An "optimal-size" adaptive window was recently proposed in [38]. Instead of maintaining window symmetry, the new approach is more concerned with the window size near the edges of image structure. This new adaptive window is structured such that all four quadrants of the window are independently adaptive, and vary in size based on an estimate of the uncorrupted signal activity in the respective window quadrant, which is derived from the local signal variance estimate $\sigma_{\hat{f}}^2 = \sigma_g^2 - \sigma_n^2$. The size of all four quadrants is adapted iteratively at each pixel location. The higher the signal activity monitored in an individual quadrant of the the more it will shrink in size at the next iteration independent of the other three, and vise versa. This continues until all four quadrants stabilize at a suitable size such that no single quadrant crosses an edge. The resulting window is optimal in the sense that for each individual pixel, the window size is allowed to grow large, even for edge pixels but does not cross over neighboring edges. This is clear from Fig. 4. The restrictions on near-edge pixels having to reduce their window size to a single pixel becomes no longer an issue.

We make use of this newly reported optimal-size adaptive window framework in minimizing our cost function E which can be given as

$$E(\hat{\mathbf{f}}) = \sum_{i \in N} \rho(g_i - \hat{f}_s, \sigma) \tag{4}$$

where $\hat{\mathbf{f}}$ is the denoised signal model, and $i \in [0, N-1]$ is a pixel located in the adaptive local neighborhood to the current pixel at position s. It should be apparent that the error argument x of $\rho(x, \sigma)$ in (4) is nothing but a local estimate of the noise signal in the adaptive region N. Thus, in minimizing this cost function, we are aiming at minimizing the noise signal in this region. The choice of this particular cost functional is motivated by the fact that our method deals with intensity discontinuities using the optimal-size adaptive windowing framework, discussed above, and assumes the outliers are only due to the noise itself, thus facilitating its removal.

Our choice of a robust estimator $\rho(x, \sigma)$ depends on the optimization scheme used to minimize the cost function. The scheme we use, which will be described momentarily, requires the estimator to be twice differentiable. The Lorentzian robust estimator satisfies this criterion. We, therefore, take $\rho(x, \sigma)$ in (4) to be the Lorentzian

$$\rho(x, \sigma) = \log\left(1 + \frac{1}{2}\left(\frac{x}{\sigma}\right)^2\right) \tag{5}$$

where σ is the scale parameter in the robust estimator formulation that controls the outlier rejection point [6]. Reducing σ will cause the estimator to reject more measurements as outliers and visa versa. Another important advantage of the Lorentzian is that it is an optimal estimator if the error distribution is Cauchy (which is an approximation of the Gaussian distribution) [32]. This is very significant as we are concerned with Gaussian distributed noise.

The influence function $\psi(x, \sigma)$ is the first derivative of $\rho(x, \sigma)$ with respect to x

$$\psi(x, \sigma) = \frac{2x}{2\sigma^2 + x^2}. \tag{6}$$

As mentioned in Section III, this function characterizes the bias that a particular measurement has on the solution [6]. The second partial derivative of $\rho(x, \sigma)$ is

$$\frac{\partial \psi(x, \sigma)}{\partial x} = \frac{2(2\sigma^2 - x^2)}{(2\sigma^2 + x^2)^2}. \tag{7}$$

The least-squares formulation of the stationarity assumption for the Wiener estimator is relatively straightforward to solve since the cost function is convex. The robust formulation of our cost function E may cause it to be nonconvex. A local minimum can, however, be obtained using a gradient-based optimization technique. We choose the successive over-relaxation minimization technique because of its rapid convergence and well defined theory [32]. The iterative equations for minimizing E over the whole image are

$$\hat{\mathbf{f}}^{t+1} = \hat{\mathbf{f}}^t - \frac{\mu}{T}\frac{\partial E}{\partial \hat{\mathbf{f}}^t} \tag{8}$$

where t is the iteration step, and $0 < \mu < 1$ is a small relaxation value that controls convergence, and is chosen empirically for each specific image to optimize the estimate.[1] The initial value $\hat{f}_s^{\,0}$, for the current pixel estimate at s, is set to the current corrupted pixel value g_s.The condition for stopping the iteration has been chosen such that the difference between the next estimate and the current estimate $|\hat{\mathbf{f}}^{t+1} - \hat{\mathbf{f}}^t|$ falls below the current value of the outlier rejection point σ indicating that any outliers have been filtered out and that the estimated pixel value belongs to the ensemble average within the adaptive window. From our experiments, which will be presented in Section V, the typical convergence occurs within five to ten iterations per pixel. After obtaining the first estimate $\hat{\mathbf{f}}$ for all the pixels in the image, the robust filter may be repeatedly applied to reduce any residual noise, as we will show in Section V.

The term T is an upper bound on the second partial derivatives of E, and is obtained when the error $x = 0$ in (7), which yields

$$T = \frac{1}{\sigma^2}. \tag{9}$$

[1]Successive over-relaxation is Newton–Raphson's minimization technique when $\mu = 1$ and $T = (\partial^2 E / \partial \hat{\mathbf{f}}^2)$.

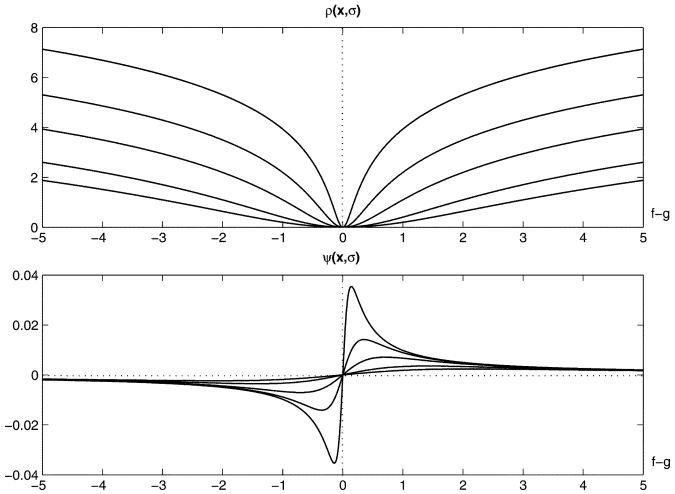

Fig. 5. Graduated nonconvexity (GNC) for (top) Lorentzian robust estimators with decreasing values of σ and (nottom) their corresponding ψ plots.

The partial derivative in (8) for a single pixel at location s is

$$\frac{\partial E}{\partial \hat{f}_s} = \sum_{i \in N} \psi(g_i - \hat{f}_s, \sigma). \tag{10}$$

The above minimization will generally converge to a local minimum. A global minimum may be found by constructing an initially convex approximation to the cost function. Formally, the cost function is convex when

$$\frac{\partial^2 E}{\partial \hat{f}_s^2} > 0 \tag{11}$$

(i.e., positive definite) at all points in the image [39]. It can be shown from (7) that E is locally convex when the maximum residual error

$$\max|g_i - \hat{f}_s| \leq \sqrt{2}\sigma. \tag{12}$$

Therefore, by choosing initial values of the σ parameters to be sufficiently large

$$\sigma = \frac{\tau_s}{\sqrt{2}} \tag{13}$$

where τ_s is the maximum expected outlier in the argument of $\rho(x)$, we are effectively blurring the cost function E so that it is approximately convex. In this range of large σ values, the ψ function is approximately linear and ρ is approximately quadratic (clearly shown in Fig. 5 for increasing values of σ). We choose τ_s to be proportional to the local estimate of the image standard deviation inside the adaptive neighborhood region N as

$$\tau_s = \zeta \cdot \sigma_N. \tag{14}$$

This formulation accounts for the nonstationary nature of the image and gives an approximate estimate of the maximum expected outlier. In flat regions of the image, σ_N will be an accurate estimate of the local noise standard deviation σ_n, while, in busy areas, $\sigma_N >> \sigma_n$ and is, in fact, approximately equal to the uncorrupted local image standard deviation σ_f. Thus, the value of τ_s is made spatially variant by changing its value based on the local sample statistics computed inside the optimal-size adaptive window of the pixel located at position s. Here, ζ is a (user-defined) weighting constant that affects the amount of smoothing and is empirically chosen to give best denoising results. Choosing a value for ζ that is too large may increase the value of σ to a point that causes the estimator to remain approximately quadratic in shape during the whole optimization process, giving rise to the standard least-squares estimator. This large value will cause more noise outliers to contribute to the least-squares-type estimate and will produce inaccurate results with excessive smoothing of high-frequency structure as in the case of the standard Wiener filter discussed earlier. On the other hand, reducing the value of ζ too much will reduce outlier contributions, but at the risk of creating an initially nonconvex cost function that gets stuck at a local minimum at the start of the optimization process.

An appropriate value for ζ, thus, needs to be chosen such that the initial minimization process uses enough samples from the adaptive window with an approximately quadratic estimator. This will reduce the initial minimization to the least-squares approach and a local minimum is obtained. Our global minimum is then gradually estimated by tracking the local minima using the GNC continuation method, described by Blake and Zisserman in [40]. The robust formulation of our cost function

TABLE I
COMPARATIVE RESULTS EXPRESSED AS MAXIMUM PSNR VALUES FOR THE VARIOUS FILTERS AT VARYING NOISE LEVELS. HIGHEST PSNR VALUES FOR EACH NOISE LEVEL ARE EMPHASIZED IN A BOLD FONT

σ_n / PSNR	Filter	Peppers	Boats	Barco	Flinstones
2 / 42.11 dB	*Robust*	**44.37**	**43.40**	44.50	**45.39**
	Bilateral	43.62	43.21	43.44	44.52
	Anis. Diff.	42.64	41.77	43.00	44.42
	BLS-GSM	43.00	42.99	**45.36**	44.14
5 / 34.15 dB	*Robust*	**40.12**	**39.28**	**39.95**	**39.60**
	Bilateral	37.85	37.58	37.21	37.47
	Anis. Diff.	38.19	37.35	36.62	37.59
	BLS-GSM	37.31	36.97	38.96	36.88
10 / 28.13 dB	*Robust*	**35.69**	**34.84**	**35.20**	**34.33**
	Bilateral	33.28	32.52	33.69	32.20
	Anis. Diff.	34.65	33.75	34.16	31.77
	BLS-GSM	33.77	33.58	34.04	32.04
15 / 24.61 dB	*Robust*	**33.30**	**32.47**	**32.89**	**31.02**
	Bilateral	31.24	30.50	31.33	29.14
	Anis. Diff.	32.60	31.68	32.27	29.38
	BLS-GSM	31.74	31.70	31.86	29.05
20 / 22.11 dB	*Robust*	**31.14**	**30.78**	**30.80**	**28.40**
	Bilateral	29.51	28.87	29.72	26.99
	Anis. Diff.	31.00	29.73	30.41	27.55
	BLS-GSM	30.26	29.38	29.04	27.00
30 / 18.59 dB	*Robust*	**28.52**	**28.11**	**28.12**	**25.07**
	Bilateral	26.94	26.52	27.21	23.88
	Anis. Diff.	28.24	27.92	27.98	24.73
	BLS-GSM	28.30	26.91	26.56	23.70

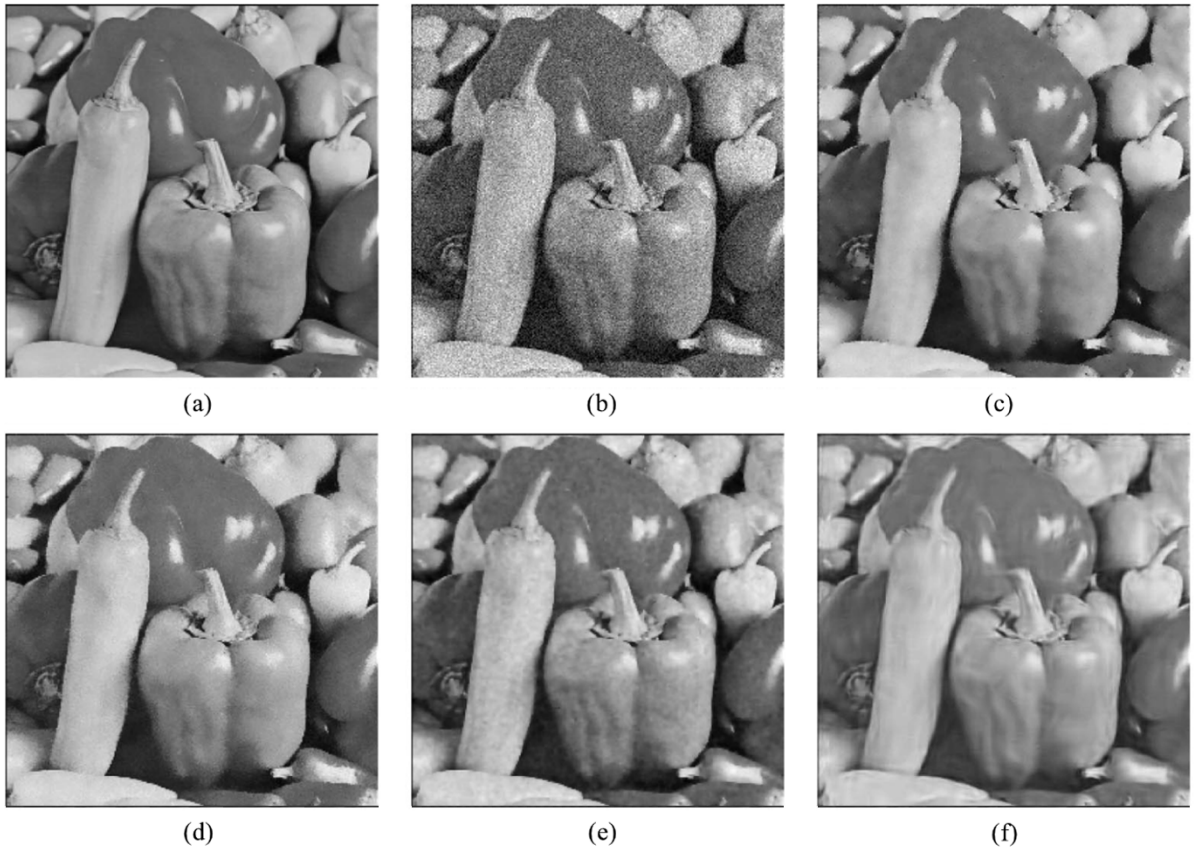

Fig. 6. (a) Ideal Peppers image of size 256×256, 256 gray levels. (b) Corrupted version of the Peppers image degraded by Gaussian white noise of standard deviation $\sigma_n = 20$, with a measured $\mathrm{PSNR} = 22.11$ dB. (c) Denoised image after two passes of the robust filter with an adaptive neighborhood window size that was allowed to grow to a maximum of $N = 5 \times 5$ with $\mu = 0.4$ and $\zeta = 0.3$ ($\mathrm{PSNR} = 31.14$ dB). (d) Bilateral filter ($\sigma_r = 30, \sigma_d = 3$) ($\mathrm{PSNR} = 29.51$ dB). (e) Anisotropic diffused image after five iterations and a conduction coefficient of 20 ($\mathrm{PSNR} = 31.00$ dB). (f) BLS-GSM filter showing too much artifacts and smoothing, but maintaining sharp edges ($\mathrm{PSNR} = 30.26$ dB).

coupled with GNC helps a global minimum to be obtained by decreasing the values of the σ parameter from one iteration to the next, which serves to gradually return the cost function to its nonconvex shape, thereby introducing back the noise outliers in the cost function (Fig. 5). These noise pixels are, however, dealt with by the robust formulation and are rejected as outliers, thus producing more accurate signal estimates compared to least-squares filtering as will be clear from the experimental results in the next section.

V. Experimental Results

In this section, experimental results are presented to show the performance of our robust denoising filter when applied to Gaussian noise corrupted digital images, and to compare its performance with other commonly used filters available in the literature.

Three nonlinear denoising approaches that have demonstrated satisfying results at smoothing noise are the wavelet domain Bayes least-squares Gaussian scale mixtures (BLS-GSM) work by Portilla *et al.* [41], [42], the bilateral filter of Tomasi and Manduchi [30], and the anisotropic diffusion technique of Perona and Malik [29]. Results from applying these techniques will be used as a comparison to results obtained from our robust denoising approach to show its relative performance in the context of nonlinear Gaussian denoising.

The reason for choosing to compare our results with anisotropic diffusion (we selected Perona and Malik's implementation [29] due to its availability[2]) is due to the fact that it is especially well adapted to the removal of zero-mean Gaussian white noise while preserving and enhancing edges by lowering the diffusivity of the diffusion equation near large image gradients. The reason for comparing with Tomasi and Manduchi's Bilateral filter is the fact that they implement a noniterative edge-preserving smoothing hybrid filter which combines both domain and range filtering, where the geometric spread σ_d in the domain is chosen based on the desired amount of low-pass filtering. A large σ_d blurs more; that is, it combines values from more distant image locations, and the photometric spread σ_r in the image range is set to achieve the desired amount of combination of pixel values, where values much closer to each other than σ_r are mixed together and values much more distant than σ_r are not. This range filtering component acts as an adaptive windowing technique. The reason for comparing our technique with the BLS-GSM method of Portialla *et al.* is due to the success this nonlinear technique has achieved in image denoising with edge preservation. The Matlab implementations of the BLS-GSM[3] and bilateral filters were obtained directly from their respective authors by e-mail.

[2]Source: http://www.csse.uwa.edu.au/~pk/Research/MatlabFns/

[3]Source: http://decsai.ugr.es/~javier/denoise/software/index.htm

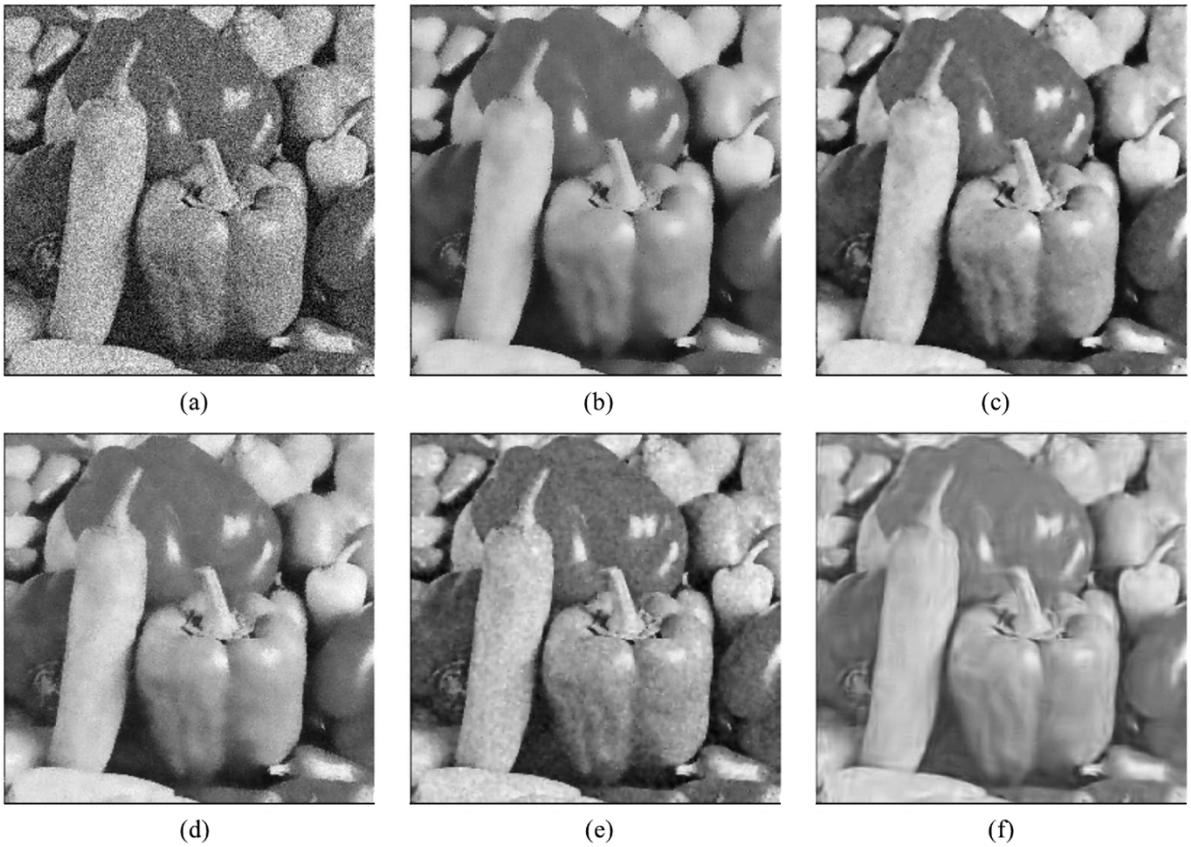

Fig. 7. (a) Corrupted version of the Peppers image in Fig. 6(a), degraded by Gaussian white noise of standard deviation $\sigma_n = 30$, with a $\mathrm{PSNR} = 18.59$ dB. (b) Denoised image after a single iteration of the robust filter with an adaptive neighborhood window size that was allowed to grow to a maximum of $N = 9 \times 9$ pixels, with $\mu = 0.4$ and $\zeta = 0.3$. ($\mathrm{PSNR} = 26.49$ dB). (c) Denoised image after 35 iterations of the robust filter with a maximum adaptive neighborhood window size of $N = 3 \times 3$ with $\mu = 0.4$ and $\zeta = 0.3$. ($\mathrm{PSNR} = 28.52$ dB). (d) Bilateral filtered image ($\sigma_r = 50$, $\sigma_d = 3$) ($\mathrm{PSNR} = 26.94$ dB). (e) Anisotropic diffused image after 6 iterations and a conduction coefficient of 30 ($\mathrm{PSNR} = 28.24$ dB). (f) BLS-GSM filter ($\mathrm{PSNR} = 28.30$ dB).

In evaluating the performance of individual filters, it is important to take into consideration both the analytical performance of the filter as well as the visual quality of the estimated images generated by the filter. The well-known mean-square-error (MSE) metric calculates the global error variance (power in the difference image) between an ideal image $\mathbf{f}$, and its estimate $\hat{\mathbf{f}}$, and has been widely used for measuring the performance of various filters [8]. The only shortcoming in an MSE metric is that it is sensitive to minor pixel variations between the ideal and estimated images that do not, in general, affect the perceived visual quality. A more robust measure of filter performance that has been widely used by the signal processing community is the peak signal-to-noise ratio given by

$$\mathrm{PSNR} = 20 \log_{10} \left(\frac{L-1}{\sigma_e} \right) \tag{15}$$

where L is the number of gray levels in the image ($L = 256$ for 8-bit images), and σ_e is the residual standard deviation in the error image given as

$$\sigma_e = \sqrt{\frac{1}{S} \sum_{s=0}^{S-1} (f_s - \hat{f}_s)^2} \tag{16}$$

for S-sized images. This measure is less sensitive to minor deviations and will be adopted for comparing the various filters. It is important to note, however, that objective measures such as the PSNR and MSE metrics are not necessarily correlated to our perception of an image. This is because methods that are least squares based are optimum in terms of MSE values without necessarily producing the best visual results. The ultimate measure of visual fidelity will have to remain our own visual perception, which is very subjective. For example, we may require extra smoothing of the denoised image when fine details are of little importance, in which case the PSNR values will not be optimum. On the other hand, we may be interested in preserving the most minute details in the restored image, at the expense of allowing a small amount of residual noise to remain after the restoration process.

Taking this subjective evaluation into account, we test our robust approach on four standard sets of natural and synthetic images commonly used for evaluation in the literature. Table I summarizes the results for all image sets at varying noise levels.

We start by showing simulation results of the performance of the adaptive window robust filter using the standard Peppers gray scale image of size 256×256 shown in Fig. 6(a), which was degraded with Gaussian noise of variance $\sigma_n^2 = 400$ and $\mathrm{PSNR} = 22.11$ dB as shown in Fig. 6(b). It is clear from Fig. 6(c) that our robust filter produces the best results both objectively in terms of its PSNR values, and subjectively by direct visual inspection. Fig. 7 shows the performance of our robust filter when denoising relatively high Gaussian

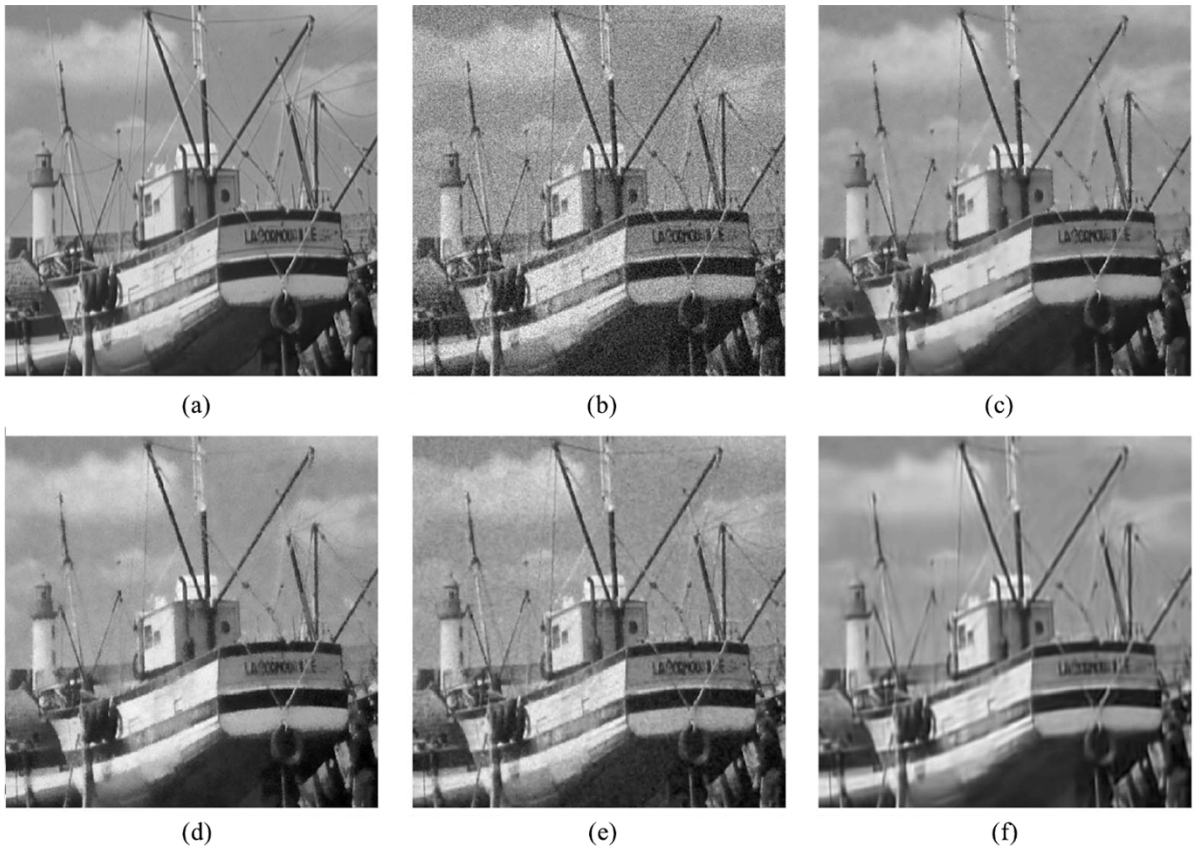

Fig. 8. (a) Original (uncorrupted) Boat image (350×350 portion of the original 512×512 image, 256 gray levels). (b) Corrupted version of the Boats image, degraded by Gaussian white noise of standard deviation $\sigma_n = 20$, with a measured $\mathrm{PSNR} = 22.11$ dB. (c) Denoised image after three iterations of the robust filter with an adaptive neighborhood window size that was allowed to grow to a maximum of $N = 5 \times 5$ with $\mu = 0.4$ and $\zeta = 0.3$ ($\mathrm{PSNR} = 30.28$ dB). (d) Bilateral filter ($\sigma_r = 30, \sigma_d = 3$) ($\mathrm{PSNR} = 28.87$ dB). (e) Anisotropic diffused image after five iterations and a conduction coefficient of 20 ($\mathrm{PSNR} = 29.73$ dB). (f) BLS-GSM filter ($\mathrm{PSNR} = 29.38$ dB).

white noise contamination of variance $\sigma_n^2 = 900$ and $\mathrm{PSNR} = 18.59$ dB. It is apparent from the figures that results of filtering using anisotropic diffusion and BLS-GSM introduce nonuniform gray-level artifacts to flat regions in the image that give a textured appearance to the objects in the image, and reduce the visual appeal of the denoised result.

We now present the results from our second experiment which involves denoising the boat image shown in Fig. 8(a) that was degraded with Gaussian white noise of variance $\sigma_n^2 = 400$. This noisy image is shown in Fig. 8(b). In this test image, the fine lines connecting the sails on the boat will clearly pose some challenges for any denoising algorithm. As we tackle this problem, we need to strike a balance between the maximum size of the adaptive window $N_{\max}$ and the number of repeated applications of the robust filter (to remove residual noise) in order to avoid any excessive smoothing. Increasing the adaptive window size allows us to repeatedly apply the robust filter less often and vise versa. The problem is complicated further as the contaminating noise variance increases. For these experiments, we have chosen the same robust filter parameter values that were used for the Peppers example ($\mu = 0.4$, and $\zeta = 0.3$). Fig. 9 shows the performance of our robust filter when denoising the boat image after relatively high noise contamination of variance $\sigma_n^2 = 900$ and $\mathrm{PSNR} = 18.59$ dB.

Finally, we present results of our robust technique in comparison with the other three denoising methods for the Barco image of Fig. 10(a) and the Flinstones image of Fig. 11(a), after relatively severe noise degradation of variance $\sigma_n^2 = 900$, shown in Figs. 10(b) and 11(b), respectively.

The above comparisons clearly show the merits of our robust technique both objectively in terms of its higher PSNR values (for the low-to-medium noise range from $\sigma_n = 5$ to $\sigma_n = 30$), compared to the other three methods at the same noise level, and subjectively by direct visual inspection in terms of overall noise removal while preserving details in the denoised image.

VI. Conclusion

This paper has presented a simple blind denoising filter based on the theory of robust statistics. A stationarity cost function was "robustified" by using the Lorentzian robust estimator instead of the nonrobust quadratic estimator and minimized using a GNC algorithm to help obtain a global minimum when the cost function is nonconvex. A newly reported adaptive windowing framework was used in the formulation of the robust filter to improve neighborhood statistical estimates. Experimental results were presented to show the performance of the new robust filter and comparisons were made with three other nonlinear denoising filters. Results have shown the robust filter to be highly effective at reducing Gaussian white noise from natural scenes while preserving fine details. In future work, the problem of recovering natural images degraded by a mixture of noise distributions

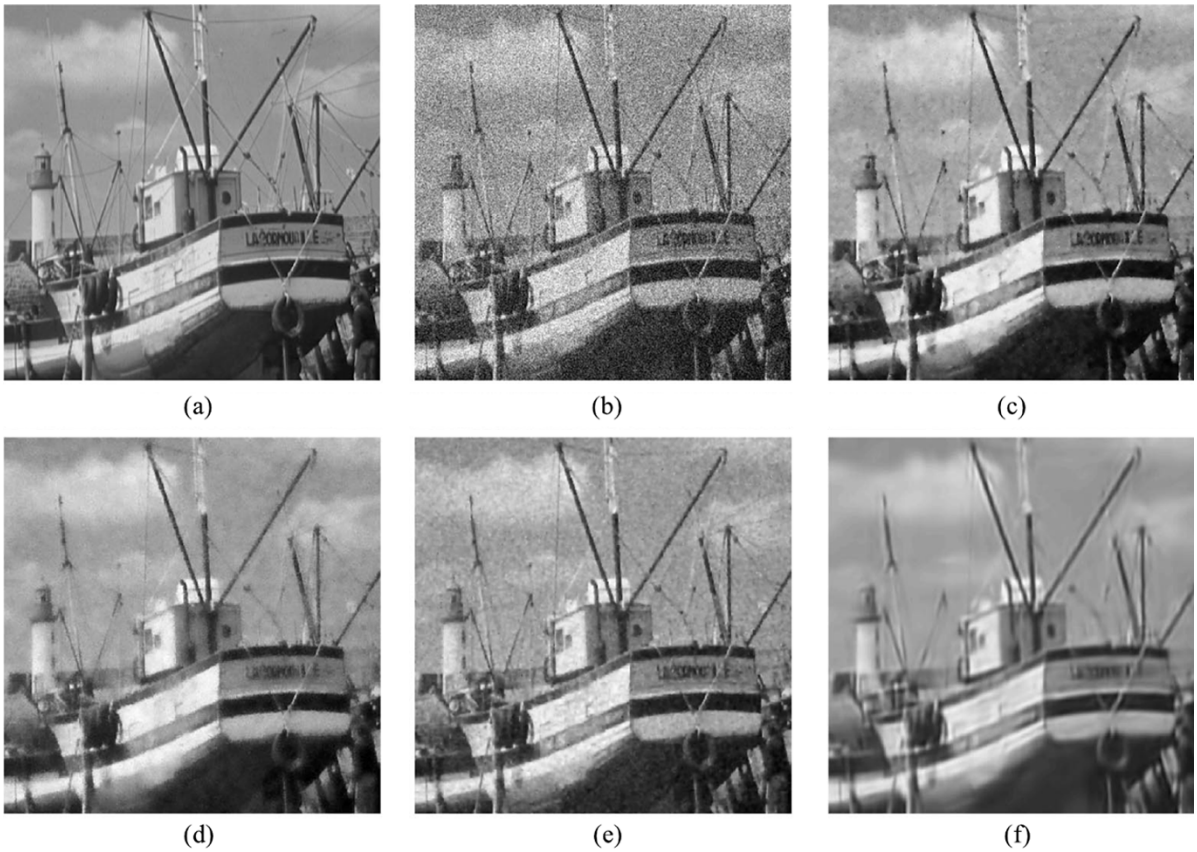

Fig. 9. (a) Ideal Boats image of size 350 × 350. (b) Corrupted version of the Boats image, degraded by Gaussian white noise of standard deviation $\sigma_n = 30$, with a measured $\mathrm{PSNR} = 18.59$ dB. (c) Denoised image after 30 iterations of the robust filter with an adaptive neighborhood window size that was allowed to grow to a maximum of $N = 3 \times 3$ with $\mu = 0.4$ and $\zeta = 0.3$ ($\mathrm{PSNR} = 28.11$ dB). (d) Bilateral filter ($\sigma_r = 50, \sigma_d = 3$) ($\mathrm{PSNR} = 26.52$ dB). (e) Anisotropic diffused image after 6 iterations and a conduction coefficient of 30 ($\mathrm{PSNR} = 27.92$ dB). (f) BLS-GSM filter ($\mathrm{PSNR} = 26.91$ dB).

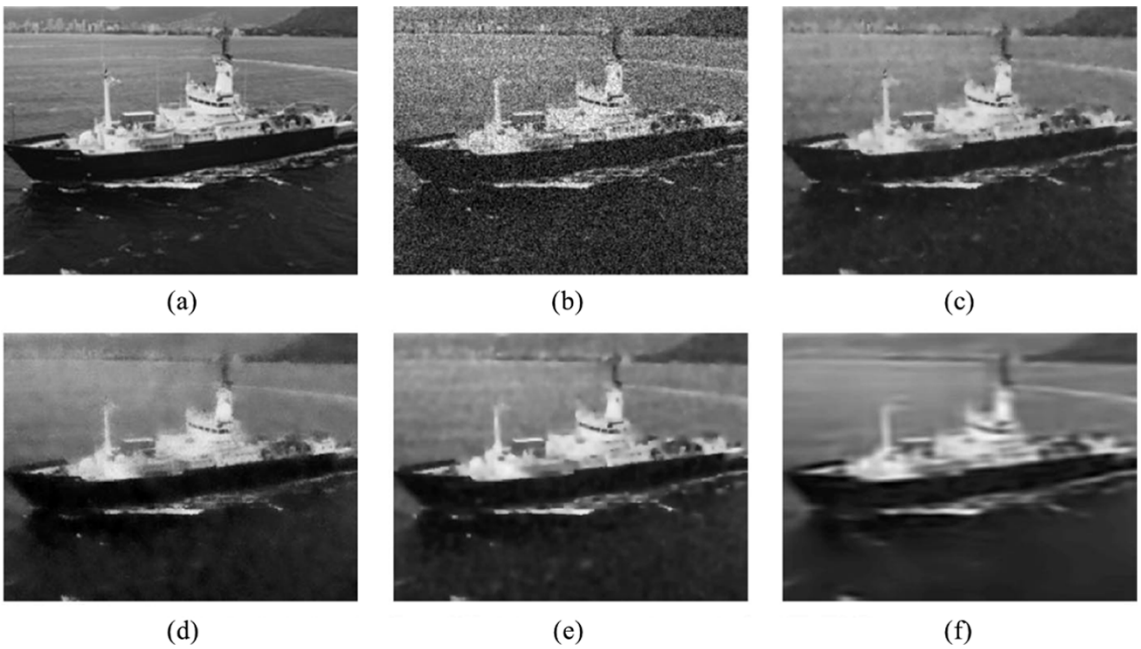

Fig. 10. (a) Ideal Barco image of size 302 × 231. (b) Corrupted version of the Barco image, degraded by Gaussian white noise of standard deviation $\sigma_n = 30$, with a measured $\mathrm{PSNR} = 18.59$ dB. (c) Denoised image after 40 iterations of the robust filter with an adaptive neighborhood window size that was allowed to grow to a maximum of $N = 3 \times 3$ with $\mu = 0.4$ and $\zeta = 0.3$ ($\mathrm{PSNR} = 28.12$ dB). (d) Bilateral filter ($\sigma_r = 60, \sigma_d = 3$) ($\mathrm{PSNR} = 27.21$ dB). (e) Anisotropic diffused image after 15 iterations and a conduction coefficient of 25 ($\mathrm{PSNR} = 27.98$ dB). (f) BLS-GSM filter ($\mathrm{PSNR} = 26.56$ dB).

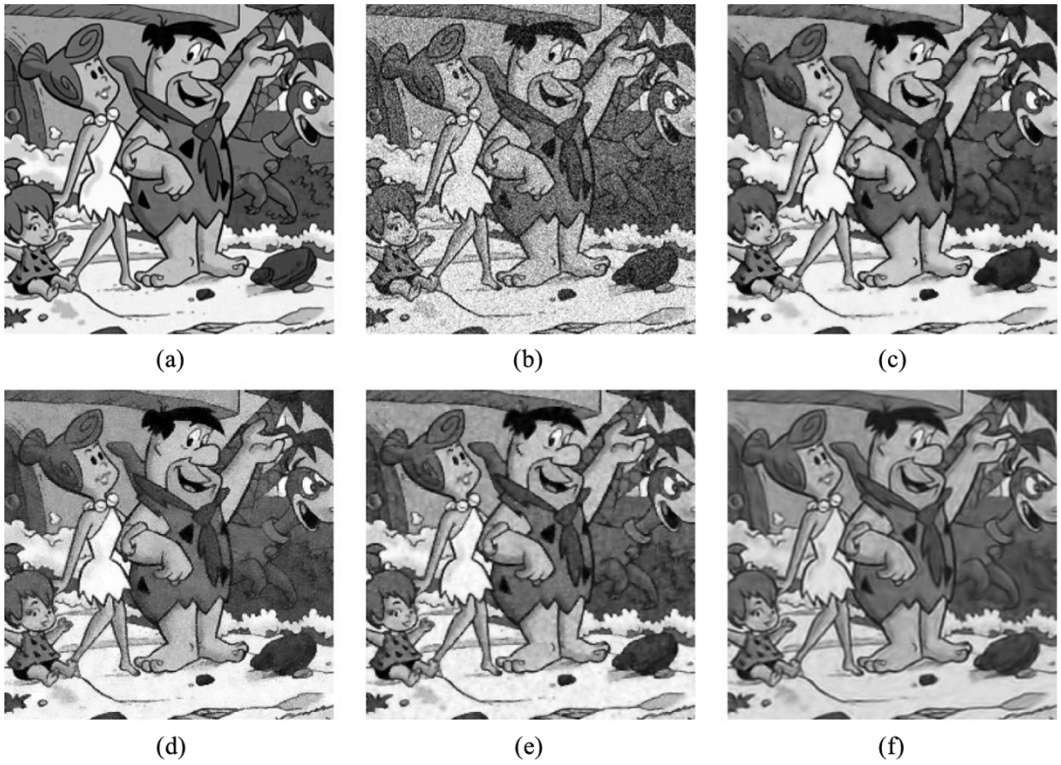

Fig. 11. (a) Ideal Flinstones image of size 256×256. (b) Corrupted version of the Flinstones image, degraded by Gaussian white noise of standard deviation $\sigma_n = 30$, with a measured $\mathrm{PSNR} = 18.59$ dB. (c) Denoised image after 35 iterations of the robust filter with an adaptive neighborhood window size that wasallowed to grow to a maximum of $N = 3 \times 3$ ($\mu = 0.4$ and $\zeta = 0.3$) ($\mathrm{PSNR} = 25.07$ dB). (d) Bilateral filter ($\sigma_r = 40, \sigma_d = 3$) ($\mathrm{PSNR} = 23.97$ dB). (e) Anisotropic diffused image after 6 iterations and a conduction coefficient of 30 ($\mathrm{PSNR} = 24.73$ dB). (f) BLS-GSM filter ($\mathrm{PSNR} = 23.70$ dB).

including impulsive and signal dependent noise will be investigated in the framework of the proposed robust statistics-based denoising filter.

REFERENCES

[1] E. Haugh, "A structural theory for the Selwyn granularity coefficient," *J. Photo. Soc.*, vol. 11, no. 65, 1963.

[2] G. Higgins and K. Stultz, "Experimental study of the RMS granularity as a function of scanning spot size," *J. Opt. Soc. Amer.*, vol. 49, no. 925, 1959.

[3] F. Naderi, "Estimation and Detection of Images Degraded by Film-Grain Noise," Univ. Southern California, Los Angeles, Tech. Rep. USCIPI 690, Sep., 1976.

[4] F. Hampel, "The influence curve and its role in robust estimation," *J. Amer. Stat. Assoc.*, vol. 69, no. 346, pp. 383–393, 1974.

[5] P. Huber, *Robust Statistics*. New York: Wiley, 1981.

[6] F. Hampel, E. Ronchetti, P. Rousseeuw, and W. Stahel, *Robust Statistics: The Approach Based on Influence Functions*. New York: Wiley, 1986.

[7] N. Wiener, *Extrapolation, Interpolation, and Smoothing of Stationary Time Series*. Cambridge, MA: MIT Press, 1942.

[8] K. Castleman, *Digital Image Processing*. Englewood Cliffs, NJ: Prentice-Hall, 1996.

[9] A. Papoulis, *Probability, Random Variables, and Stochastic Processes*, 3rd ed. New York: McGraw-Hill, 1991.

[10] A. Hillery and R. Chin, "Iterative wiener filters for image restoration," *IEEE Trans. Signal Process.*, vol. 39, no. 8, pp. 1892–1899, Aug. 1991.

[11] M. Sonka, V. Hlavac, and R. Boyle, *Image Processing, Analysis, and Machine Vision*, 2 ed. Boston, MA: PWS-Kent, 1999.

[12] S. Rajala and R. DeFigueiredo, "Adaptive nonlinear image restoration be a modified Kalman filtering approach," *IEEE Trans. Acoust., Speech, Signal Process.*, vol. ASSP-29, no. 5, pp. 1033–1042, Oct. 1981.

[13] C. Pomalaza-Raez and C. McGillem, "An adaptive, nonlinear edge-preserving filter," *IEEE Trans. Acoust., Speech, Signal Process.*, vol. ASSP-32, no. 3, pp. 571–576, Jun. 1984.

[14] R. Paranjape, T. Rabie, and R. Rangayyan, "Image restoration by adaptive-neighborhood noise subtraction," *Appl. Opt.*, vol. 33, no. 14, pp. 2861–2869, May 1994.

[15] A. Flaig, G. R. Arce, and K. E. Barner, "Affine order statistic filters: A date-adaptive filtering framework for nonstationary signals," in *Proc. IEEE Int. Conf. Acoustics, Speech, and Signal Processing*, 1997, pp. 2145–2148.

[16] J. Park, W. Song, and W. Pearlman, "Speckle filtering of sar images based on adaptive windowing," *Proc. Inst. Elect. Eng.*, vol. 146, no. 4, pp. 191–197, 1999.

[17] M. Black, D. Fleet, and Y. Yacoob, "Robustly estimating changes in image appearance," *Comput. Vis. Image Understand.*, vol. 78, pp. 8–31, 2000.

[18] H. Eng and K. Ma, "Noise adaptive soft-switching median filter," *IEEE Trans. Image Process.*, vol. 10, no. 2, pp. 242–251, 2001.

[19] R. Kashyap and K. Eom, "Robust image modeling techniques with an image restoration application," *IEEE Trans. Acoust., Speech, Signal Process.*, vol. ASSP-36, no. 8, pp. 1313–1325, Aug. 1988.

[20] A. Hamza and H. Krim, "Image denoising: A nonlinear robust statistical approach," *IEEE Trans. Signal Process.*, vol. 49, no. 12, pp. 3045–3054, Dec. 2001.

[21] S. Sardy, P. Tseng, and A. Brace, "Robust wavelet denoisiing," *IEEE Trans. Signal Process.*, vol. 49, no. 6, pp. 1146–1152, Jun. 2001.

[22] V. I. Ponomaryov, F. J. G. Funes, O. B. Pogrebnyak, and L. N. De Rivera, "Denoising robust image filter with retention of small-size details in presence of complex noise mixture," in *Proc. SPIE Conf. Viual Communications and Image Processing*, vol. 4671 II, San Jose, CA, Jan. 2002, pp. 877–887.

[23] M. Black, G. Sapiro, D. Marimont, and D. Heeger, "Robust anisotropic diffusion," *IEEE Trans. Image Process.*, vol. 7, no. 3, pp. 421–432, Mar. 1998.

[24] S. C. Zhu and D. Mumford, "Prior learning and gibbs reaction-diffusion," *IEEE Pattern Anal. Mach. Intell.*, vol. 19, no. 11, pp. 1236–1250, Nov. 1997.

[25] J. Weickert, "Applications of nonlinear diffusion in image processing and computer vision," in *Proc. Algoritmy Acta Math. Univ. Comenianae*, vol. LXX, 2001, pp. 33–50.

[26] P. Mrazek, "Nonlinear diffusion for image filtering and monotonicity enhancement," Ph.D. dissertation, Dept. Comput. Eng., Czech Tech. Univ., Prague, Czech Republic, Jun. 2001.

[27] D. Tschumperl and R. Deriche, "Vector-valued image regularization with pde's: A common framework for different applications," presented at the IEEE Conf. Comput. Vision Pattern Recognit., Madison, WI, Jun. 2003.
[28] P. Perona and J. Malik, "Scale-space and edge detection using anisotropic diffusion," in *Proc. IEEE Computer Society Workshop on Computer Vision*, 1987, pp. 16–27.
[29] ——, "Scale-space and edge detection using anisotropic diffusion," *IEEE Pattern Anal. Mach. Intell.*, vol. 12, no. 7, pp. 629–639, Jul. 1990.
[30] C. Tomasi and R. Manduchi, "Bilateral filtering for gray and color images," presented at the IEEE Int. Conf. Computer Vision, Bombay, Maharashtra, India, 1998.
[31] D. Barash and D. Comaniciu, "A common framework for nonlinear diffusion, adaptive smoothing, bilateral filtering and mean shift," *Image Video Comput.*, vol. 22, no. 1, pp. 73–81, 2004.
[32] M. Black, "Robust incremental optical flow," Dept. Comput. Sci., Yale Univ., Tech. Rep. YALEU/DCS/RR-923, 1992.
[33] P. Rousseeuw and A. Leroy, *Robust Regression and Outlier Detection*. New York: Wiley, 1987.
[34] M. Black and A. Rangarajan. The outlier process: Unifying line processes and robust statistics. presented at IEEE Conf. Computer Vision and Pattern Recognition. [Online]. Available: citeseer.nj.nec.com/black94outlier.html
[35] P. Chan and J. Lim, "One-dimensional processing for adaptive image restoration," *IEEE Trans. Acoust., Speech, Signal Process.*, vol. ASSP-33, no. 1, pp. 117–129, Feb. 1985.
[36] Y. Boykov, O. Veksler, and R. Zabih, "A variable window approach to early vision," *IEEE Trans. Pattern Anal. Mach. Intell.*, vol. 20, no. 12, pp. 1283–1294, Dec. 1998.
[37] K. Egiazarian, V. Katkovnik, and J. Astola, "Adaptive window size image denoising based on ici rule," in *Proc. ICASSP*, May 2001, pp. 1869–1872.
[38] T. Rabie, "Adaptive hybrid mean and median filtering of high-iso long-exposure sensor noise for digital photography," *SPIE J. Electron. Imag.*, vol. 13, no. 2, pp. 264–277, Apr. 2004.
[39] R. Rockafellar, *Convex Analysis*. Princeton, NJ: Princeton Univ. Press, 1970.
[40] A. Blake and A. Zisserman, Eds., *Visual Reconstruction*. Cambridge, MA: MIT Press, 1987.
[41] J. Portilla, V. Strela, M. Wainwright, and E. Simoncelli, "Image denoising using Gaussian scale mixtures in the wavelet domain," Courant Inst. Math. Sci., New York Univ., New York, Tech. Rep. TR2002-831, Sep. 29, 2002.
[42] ——, "Image denoising using scale mixtures of Gaussian in the wavelet domain," *IEEE Trans. Image Process.*, vol. 12, no. 11, pp. 1338–1351, Nov. 2003.

Tamer Rabie (S'89–M'99–SM'03) received the M.Sc. degree in adaptive image restoration from the Department of Electrical and Computer Engineering, University of Calgary, Calgary, AB, Canada, in 1993, and the Ph.D. degree in active computer vision applied to dynamic virtual environments from the Department of Electrical and Computer Engineering, University of Toronto, Toronto, ON, Canada, in January 1999.

During the period from January 2000 to August 2001, he held an Assistant Professor appointment with the Department of Electrical and Computer Engineering, Ryerson University, Toronto. He has been an Assistant Professor with the College of Information Technology, UAE University, Al-Ain, United Arab Emirates, since August 2001. He has also been an Adjunct Professor at the University of Toronto's Intelligent Transportation Systems Centre since May 2000, conducting collaborative research work in active computer vision-based traffic surveillance and control. His current research interests include digital image processing, computer vision, augmented reality, and their applications in the field of intelligent transportation systems.

Dr. Rabie has an active membership in the IEEE Signal Processing Society and the Professional Engineers of Ontario (PEO) Association in Canada. He is a reviewer for the International Association of Science and Technology for Development (IASTED), and has been appointed as a member of the technical committee on computer vision and the technical committee on image processing since September 2001. He has also served as an area chair and reviewer for the 6th IEEE Workshop on Applications of Computer Vision (WACV) and is a permanent member of the advisory and program committee for the International Conference on Image Analysis and Recognition (ICIAR).